Chinese Journal of
POLYMER SCIENCE

ARTICLE

https://doi.org/10.1007/s10118-020-2374-1
Chinese J. Polym. Sci. **2020**, *38*, 599–610

Enhanced Crystallization Rate of Poly(L-lactide)/Hydroxyapatite-graft-poly(D-lactide) Composite with Different Processing Temperatures

Min Wang, Lei-Chu You, Yu-Qi Guo, Ni Jiang, Zhi-Hua Gan, and Zhen-Bo Ning*

State Key Laboratory of Organic-Inorganic Composites, Beijing Laboratory of Biomedical Materials, College of Life Science and Technology, Beijing University of Chemical Technology, Beijing 100029, China

Electronic Supplementary Information

Abstract Hydroxyapatite-graft-poly(D-lactide) (HA-*g*-PDLA) was synthesized by ring-opening polymerization with HA as initiator and stannous octanoate ($Sn(Oct)_2$) as catalyst. Thermogravimetric analysis (TGA) and Fourier transform infrared spectroscopy (FTIR) results indicate that PDLA chains are successfully grafted onto HA particles by covalent bond. Under two different processing temperatures (190 and 230 °C), the effect of the grafted PDLA chains on the crystallization behavior of poly(L-lactide)/HA-*g*-PDLA (PLLA/HA-*g*-PDLA) composite was investigated in the current study, comparing to neat PLLA and its four composites (PLLA/HA, PLLA/HA-*g*-PLLA, PLLA/PDLA, and PLLA/HA/PDLA). The crystallization rate of PLLA/HA-*g*-PDLA composite is highly enhanced comparing to PLLA, PLLA/HA and PLLA/HA-*g*-PLLA composites in which there are no stereocomplex (SC) crystallites. In addition, when the processing temperature rises from 190 °C to 230 °C, the acceleration of PLLA crystallization in PLLA/HA-*g*-PDLA composite is not influenced so much as other composites containing SC crystallites, such as PLLA/HA/PDLA or PLLA/PDLA. The differential scanning calorimetry (DSC) results demonstrate that even without SC crystallites, the crystallization of PLLA can still be accelerated a lot in this composite. This may be related to the interaction between the grafted PDLA chains and the amorphous PLLA chains in PLLA/HA-*g*-PDLA composite. The isothermal crystallization kinetics studies indicate that the nature of nucleation and crystal growth of PLLA/HA-*g*-PDLA composite are more likely 3D crystalline growth with heterogeneous nucleation mode, which are different from PLLA or other composites. This investigation could shed new light on the application of PLLA/HA composites.

Keywords HA particles; Stereocomplexation; Composite; Crystallization

Citation: Wang, M.; You, L. C.; Guo, Y. Q.; Jiang, N.; Gan, Z. H.; Ning, Z. B. Enhanced crystallization rate of poly(L-lactide)/hydroxyapatite-graft-poly(D-lactide) composite with different processing temperatures. *Chinese J. Polym. Sci.* **2020**, *38*, 599–610.

INTRODUCTION

Poly(lactide) (PLA) has been well investigated for its excellent properties, such as biodegradability, biocompatibility, and desired mechanical properties.[1–3] It has therefore been applied to the preparation of controlled release drugs, tissue engineering, and bone fracture fixation.[4–6] PLA possesses three stereochemical forms: poly(L-lactide) (PLLA), poly(D-lactide) (PDLA), and poly(D,L-lactide) (PDLLA). PLLA and PDLA are semicrystalline, while PDLLA is amorphous. PLLA is the most widely used in the three stereochemical forms, because the production of PDLA is expensive and PLLA owns higher mechanical strength than amorphous PDLLA.[7,8] However, the slow crystallization rate of PLLA restricts its extensive application.[9,10]

The combination of hydroxyapatite (HA) particles and PLA is an effective way to modify PLA.[11–13] HA owns the general formula of $Ca_{10}(PO_4)_6(OH)_2$. Because of its biocompatibility and similarity to the mineral phase of native bone, it has been widely used for bone tissue engineering. HA is often blended with PLA to combine the good bone binding, bone regeneration and osteoconductivity of HA with the easy processing properties of PLA.[14,15] It can delay the early degradation of PLA, overcome the formation of the acidic environment and improve the mechanical properties of the material.[16] However, due to the lack of interaction between HA particles and PLA matrix, it is difficult for HA particles to disperse uniformly in PLA matrix, and the weak interfacial adhesion can be easily destroyed after implantation, resulting in a rapid reduction in mechanical properties.[17] Therefore, improving the interaction between HA particles and PLA matrix is critical to the mechanical properties of HA/PLA composites.

The *in situ* grafting polymerization method is an effective way to avoid the aggregation of inorganic particles, and it can introduce PLA chains to the surface of HA particles through covalent bonding. The hydroxyapatite-graft-polylactide (HA-*g*-PLA) particles exhibit improved adhesion to PLA matrix, and HA-*g*-PLA/PLA composite shows greater enhancement of tensile strength and elastic modulus comparing to PLA/HA composite.[18–20] Furthermore, Huang reported that if PDLA chains are grafted to HA surface, PLA stereocomplexation can

* Corresponding author, E-mail: zbning@mail.buct.edu.cn

Received September 26, 2019; Accepted November 25, 2019; Published online December 30, 2019

be formed at the interface of HA particles, and the tensile strength and elongation of the composite increased more significantly than PLLA/HA-*g*-PLLA.[21] In this work, the crystallization of the PLLA/HA-*g*-PDLA composite was investigated with a melting temperature of 240 °C, which was higher than the melting temperature of SC crystallites, so there would be a competition between the formation of PLLA homocrystallites and SC crystallites during the crystallization process. However, if the melting temperature was below the melting temperature of SC crystallites, the crystallization of the composite would be different, because the processing temperature (or melting temperature) has a significant effect on the acceleration of crystallization rate of PLLA/PDLA composite.[22] When the processing temperature is higher than the melting temperature of SC crystallites, the nucleating effect of the SC crystallites on PLLA crystallization will be reduced comparing to a processing temperature below the melting temperature of SC crystallites.[23] Therefore, if different processing temperatures are used in the composite, the PDLA chains grafted onto HA particles will also play different roles in the crystallization of the composite. Moreover, as PDLA chains are grafted onto the HA particles, the surface of the HA particles can affect the interaction between the grafted PDLA chains and the PLLA chains, in this way, the stereocomplexation in the composite will also be affected. This effect may also be different when the processing temperature changes, so it is necessary to investigate the crystallization of the PLLA/HA-*g*-PDLA composite with different processing temperatures, which will lead to different properties of the composites.

In the present work, HA-*g*-PDLA was synthesized and blended with an equal mass of PLLA to form SC crystallites on the surface of HA particles. We used different processing temperatures (190 and 230 °C), which are below and above the melting temperature of SC crystallites, respectively. The crystallization behavior of PLLA/HA-*g*-PDLA composite was investigated for understanding the formation of the SC crystallites at the interface of HA particles and their effect on the PLLA crystallization in the composite. Mechanism for the acceleration effect in PLLA/HA-*g*-PDLA composite will be discussed by comparing to PLLA and its other four composites (PLLA/HA, PLLA/HA-*g*-PLLA, PLLA/PDLA, PLLA/HA/PDLA).

EXPERIMENTAL

Materials

D-lactide (DLA) (99% optical purity), L-lactide (LLA) (99% optical purity) and PLLA ($M_n = 7.02 \times 10^4$ g/mol, $M_w = 8.84 \times 10^4$ g/mol, PDI = 1.26) were purchased from PURAC Biomaterials (Netherlands) and the monomors were purified by recrystallization from anhydrous ethyl acetate and then dried in a vacuum oven for 72 h before use. PDLA (M_n = 8000 g/mol, M_w = 8600 g/mol, PDI = 1.08) used in the composite was sythesized in our lab according to the molecular weight of the grafted PDLA in HA-*g*-PDLA. Toluene (AR grade, Sinopharm Chemical Reagent Beijing Co., Ltd.) was distilled in the presence of metallic sodium and benzophenone. Stannous octoate ($Sn(Oct)_2$) (Sigma-Aldrich) was dissolved in dehydrated toluene prior to use. Hydroxyapatite (≥ 97% phase purity, Sigma-Aldrich) was fully dried at 100 °C in a vacuum oven before use. Ethylene glycol (AR grade, Sinopharm Chemical Reagent Beijing Co., Ltd.) was dehydrated over calcium hydroxide and then distilled under reduced pressure.

Surface Grafting of HA *via in Situ* Polymerization

The grafting polymerization of DLA onto HA particles was carried out by using 2.5 g of HA as initiator and 7.5 g of DLA as monomor in the presence of 120 μL of $Sn(Oct)_2$ in toluene (0.905 mol/L) and 50 mL of toluene; it was kept under an argon atmosphere and anhydrous conditions at 120 °C for 48 h. The dispersion-centrifugation-collection cycle reported in previous studies was repeated seven times to remove the free PDLA chains. At last, the HA-*g*-PDLA powders were vacuum-dried for 1 week to a constant weight. HA-*g*-PLLA was synthesized and purified in the same way.

Synthesis of PDLA

The polymerization of PDLA was carried out as follows. A dried glass reaction tube was degassed and purged three times with argon. Then, 2 g of DLA, 12.2 μL of ethylene glycol, 8.29 μL of $Sn(Oct)_2$ in toluene (0.905 mol/L), and 4 mL of toluene were introduced into the reaction tube. The reaction was carried out at 120 °C for 2 days. The reaction mixture was dissolved in dichloromethane (CH_2Cl_2) and then precipitated in excess of methanol. The product was dried under vacuum for 1 week before further characterization.

Preparation of Composites

PLLA/HA, PLLA/HA-*g*-PLLA, and PLLA/HA-*g*-PDLA composites were prepared by the solution-casting method as follows. Modified or unmodified HA particles were uniformly dispersed in chloroform under magnetic stirring, then the above HA-containing suspensions were added into the chloroform solution of PLLA. The weight ratio of PLLA to modified or unmodified HA particles in the mixture is 1/1. The mixture solution of PDLA/PLLA was prepared by mixing the chloroform solution of PLLA and PDLA. Chloroform was then removed by evaporation and these composites were vacuum-dried. HA/PDLA/PLLA composite and PDLA/PLLA composite were prepared using the same method.

Analysis and Characterization

The ^{1}H-NMR spectra of polymerization products were recorded on a Varian 400MHz spectrometer at room temperature with $CDCl_3$ as solvent.

Fourier-transform infrared (FTIR) measurements of the thin films were performed using a Nicolet 6700 FTIR (USA) spectrometer equipped with an attenuated total reflectance (ATR). The spectra were obtained by adding 32 scans at a resolution of 4 cm^{-1}.

The amount of grafted organic materials was determined using a thermo-gravimetric analyzer (Pyris 1, Perkin Elmer). The measurement was performed at a heating rate of 5 °C/min from room temperature to 600 °C (in air). The amount of surface grafted PLA was determined by the percentage of weight loss during heating.

Differential scanning calorimetry (DSC) curves of all samples (about 5 mg, encapsulated in aluminum pans) were recorded on a Pyris Diamond DSC with a nitrogen atmosphere as circulating atmosphere. The calibration was performed with indium and hexatriacontane. For the first heating curves, the specimens were heated to 230 °C at a rate

https://doi.org/10.1007/s10118-020-2374-1

of 10 °C/min. For non-isothermal crystallization, specimens were first melted at 190 or 230 °C for 3 min to erase the thermal history, then cooled to 50 °C at a rate of 5 °C/min, and second heated to 230 °C at a rate of 10 °C/min. For isothermal crystallization curves, the specimens were first melted at 190 or 230 °C for 3 min to erase the thermal history, then cooled to 140 °C at a rate of 45 °C/min. After holding at 140 °C for 1 h, the specimens were then heated to 230 °C at a rate of 10 °C/min.

For observation of the spherulitic morphology of PLLA composites, the films between microscope coverslips were prepared by melting at 190 or 230 °C for 3 min and then quenching to the designed temperature in a Linkam THMS-600 hot stage for isothermal crystallization. The films were observed between crossed polarizers in an optical microscope (Leica DMLP, Leica Germany) equipped with a camera system.

The crystal structure and crystallinity of PLLA composites were measured by wide-angle X-ray diffraction (WAXD). The WAXD patterns of melt-crystallized films were recorded at room temperature on a Rigaku D/Max-2500 diffractometer with a nickel-filtered Cu Kα radiation (wavelength λ = 0.154 nm, 40 kV, and 110 mA) in the 2θ range from 5° to 40° at a scanning step of 0.02°. The films used in the experiment were obtained by quenching in liquid nitrogen after melting at 190 or 230 °C for 3 min.

RESULTS AND DISCUSSION

Synthesis and Characterization of HA-*g*-PDLA

Scheme 1 shows the synthesis route to HA-*g*-PDLA *via in situ* polymerization. The grafting polymerization was carried out under the catalysis of $Sn(Oct)_2$. To confirm the successful synthesis of HA-*g*-PDLA, the IR spectra of HA and HA-*g*-PDLA are shown in Fig. 1(a). The IR bands at 566, 605, 963, 1040, 1090 cm^{-1} are attributed to phosphate group,[24,25] and 873, 1420 and 1455 cm^{-1} are related to the carbonate group.[26] There are some weak bands in the range of 2200–2000 cm^{-1} due to POH vibration in crystal lattice.[27] After surface grafting, a new absorption band appears at 1760 cm^{-1} belonging to the carbonyl group of PLA on the surface of HA-*g*-PLA. This means that the PLA chains are grafted onto the surface of HA particles. At the same time in Fig. S1 (in the electronic supplementary information, ESI), the improved dispersion of HA-*g*-PLA in chloroform confirms again the successful grafting of PDLA.

The grafting rate of HA-*g*-PDLA is determined by the thermal gravimetric analysis of neat HA and HA-*g*-PDLA (washing with chloroform and centrifuging for seven times) in Fig. 1(b). The value of the mass loss of HA-*g*-PDLA is 3.0% when the temperature rises to 600 °C, which is greater than that of neat HA (0.8%). This means that a small amount of PDLA chains (2.2% mass fraction of HA-*g*-PDLA) are grafted on HA particles.[18] It should be noted that free PDLA molecular chains which were not grafted onto the surface of the HA particles were removed completely from the sample, and it is confirmed in Fig. S2 (in ESI). After seven cycles of dispersion-centrifugation-collection, the mass loss of the dried HA-*g*-PDLA is almost the same as the sample of dispersing and centrifuging for five times, indicating that seven cycles are enough for removing the free PDLA chains in the product. It is assumed that the avarage molecular weight of PDLA grafted onto HA particles is identical to that of the free PDLA chains in

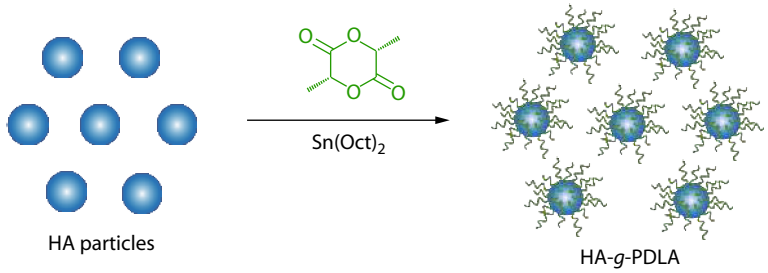

Scheme 1 Synthesis of HA-*g*-PDLA *via in situ* polymerization.

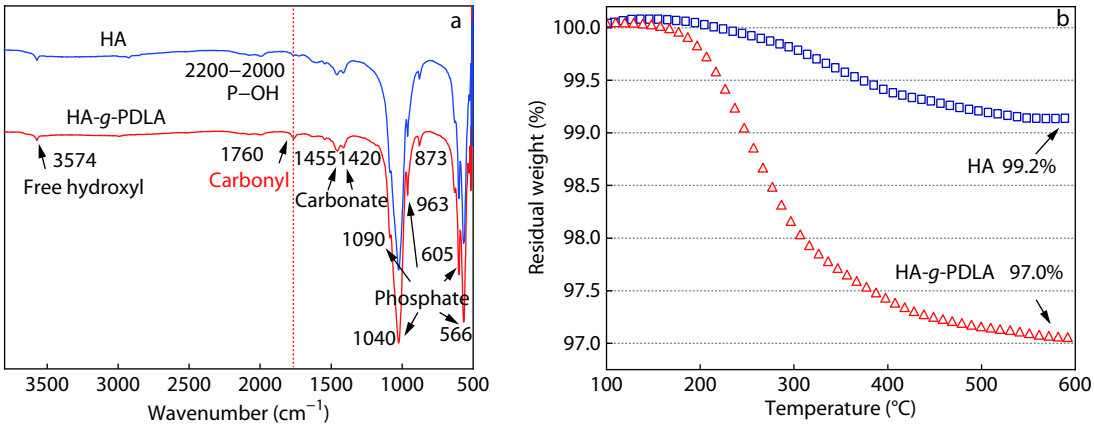

Fig. 1 Confirmation of successful grafting of PDLA chains onto HA particles by (a) FTIR spectra and (b) TGA analysis.

https://doi.org/10.1007/s10118-020-2374-1

PLLA/HA-*g*-PDLA composite, and it is calculated to be 8100 according to the method in previous studies.[28]

Composition Control of the Different PLLA Composites

In PLLA/HA-*g*-PDLA composite, PLLA homocrystallization may be affected by both HA particles and SC crystallites formed by the grafted PDLA and PLLA chains in the composite. As a result, in order to understand the different roles of HA particles and SC crystals in the crystallization process, four composites including PLLA/HA, PLLA/HA-*g*-PLLA, PLLA/HA/PDLA, and PLLA/PDLA were prepared and their crystallization behaviors were investigated for comparison. Table 1 shows the composition of PLLA and its five composites. Referring to the weight ratio of PDLA to PLLA or HA particles in PLLA/HA-*g*-PDLA composite, which is about 2.2/100, the composition of other composites was controlled.

Table 1 Code names and composition of the composite categories.

Code	Sample composition (wt%)				
	HA	PDLA	HA-*g*-PLLA	HA-*g*-PDLA	PLLA
PLLA	–	–	–	–	100
PLLA/HA	50	–	–	–	50
PLLA/HA-*g*-PLLA	–	–	50	–	50
PLLA/PDLA	–	2.2	–	–	97.8
PLLA/HA/PDLA	48.9	1.1	–	–	50
PLLA/HA-*g*-PDLA	–	–	–	50	50

Selection of the Processing Temperatures

It is well known that the PLLA homocrystallization behavior in the blend of PLLA and PDLA is highly dependent on the relationship between the processing temperature and the melting zone (T_{mz}) of SC crystallites. If the processing temperature is below T_{mz}, which means SC crystallites are non-melted, these crystallites can serve as effective nucleators for PLLA homocrystallization. On the other hand, if the processing temperature is above T_{mz}, SC crystallites will be melted, and the homocrystallization of PLLA will be affected in a different way as the SC crystallites may also be in the recrystallization process during PLLA crystallization.[29] As discussed above, in this work two different processing temperatures, which are above and below the T_{mz} of SC crystallites respectively, were selected to further investigate the influence of the HA particles grafted by PDLA chains on PLLA crystallization in the composite.

The T_{mz} of SC crystallites is obtained from the first melting curve in Fig. 2(a), and the arrow marks show the melting peaks of the SC crystallites. The melting peaks of the stereocomplex crystallites appear in the composites containing PDLA chains, such as PLLA/PDLA composite, PLLA/HA/PDLA composite and PLLA/HA-*g*-PDLA composite. The results show that homocrystallites are completely melted at 185 °C, and T_{mz}s of stereocomplex crystallites in PLLA/HA-*g*-PDLA, PLLA/HA/PDLA, and PLLA/PDLA composite are 192 °C to 200 °C, 200 °C to 216 °C, and 200 °C to 220 °C, respectively. Based on these results, 190 and 230 °C were selected as two different processing temperatures, which are above and below the T_{mz} of SC crystallites, respectively. In addition, the crystallization enthalpies of the stereocomplex crystallites ($\Delta H_{m,sc}$) are 2.7, 1.7, and 0.3 J/g for PDLA/PLLA, HA/PDLA/PLLA, and PLLA/HA-g-PDLA composite, respectively, reflecting the decrease in the amount of SC crystallites formed in these composites.

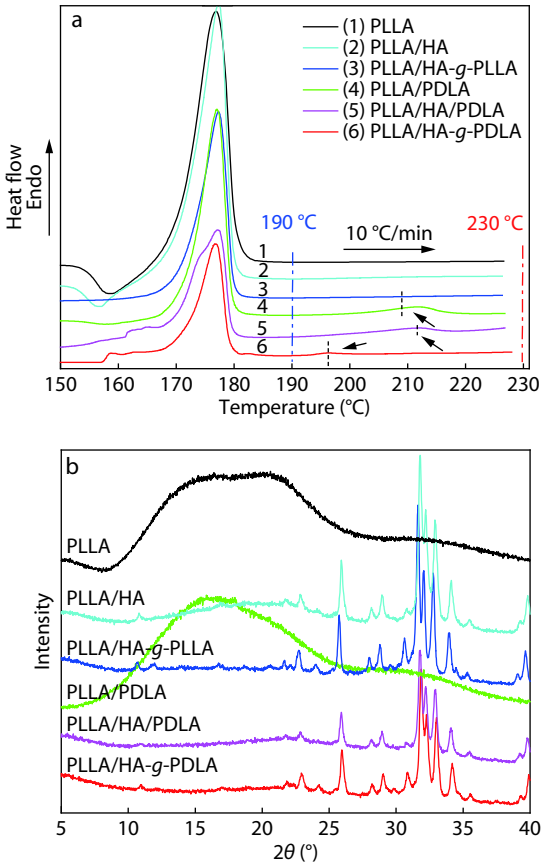

Fig. 2 Selection of the processing temperatures by DSC and WAXD results. (a) DSC curves of PLLA and its composites during the first heating run. (b) WAXD results of PLLA and its composites which were quenched in liquid nitrogen after melting at 190 °C for 3 min.

The WAXD results of PLLA and its composites, which were quenched in liquid nitrogen after melting at 190 °C for 3 min, are shown in Fig. 2(b). Neat PLLA and PLLA/PDLA show large broad halo amorphous peaks at 2θ = 16.5° and around 10.0° to 25.0°. For PLLA/HA, PLLA/HA-*g*-PLLA, PLLA/HA/PDLA, and PLLA/HA-*g*-PDLA composites, the scattering peaks related to the HA particles can be observed. These results mean the PLLA crystallites melt completely in these composites when the temperature rises to 190 °C. However, as the content of the PDLA is very low, it is difficult to observe the scattering peaks related to the SC crystallites in the WAXD results. When the processing temperature rises to 230 °C, the results are similar to those in Fig. 2(b).

Processing Temperature below T_{mz} of SC Crystallites

Non-isothermal crystallization and isothermal crystallization after melting at 190 °C were investigated in Fig. 3. The quantitative analyses of the thermal properties of PLLA and its composites during non-isothermal crystallization and subsequent heating process are tabulated in Table 2. Fig. 3(a) shows the non-isothermal crystallization curves of PLLA and its composites when the processing temperatures is 190 °C. Figs. 3(b)

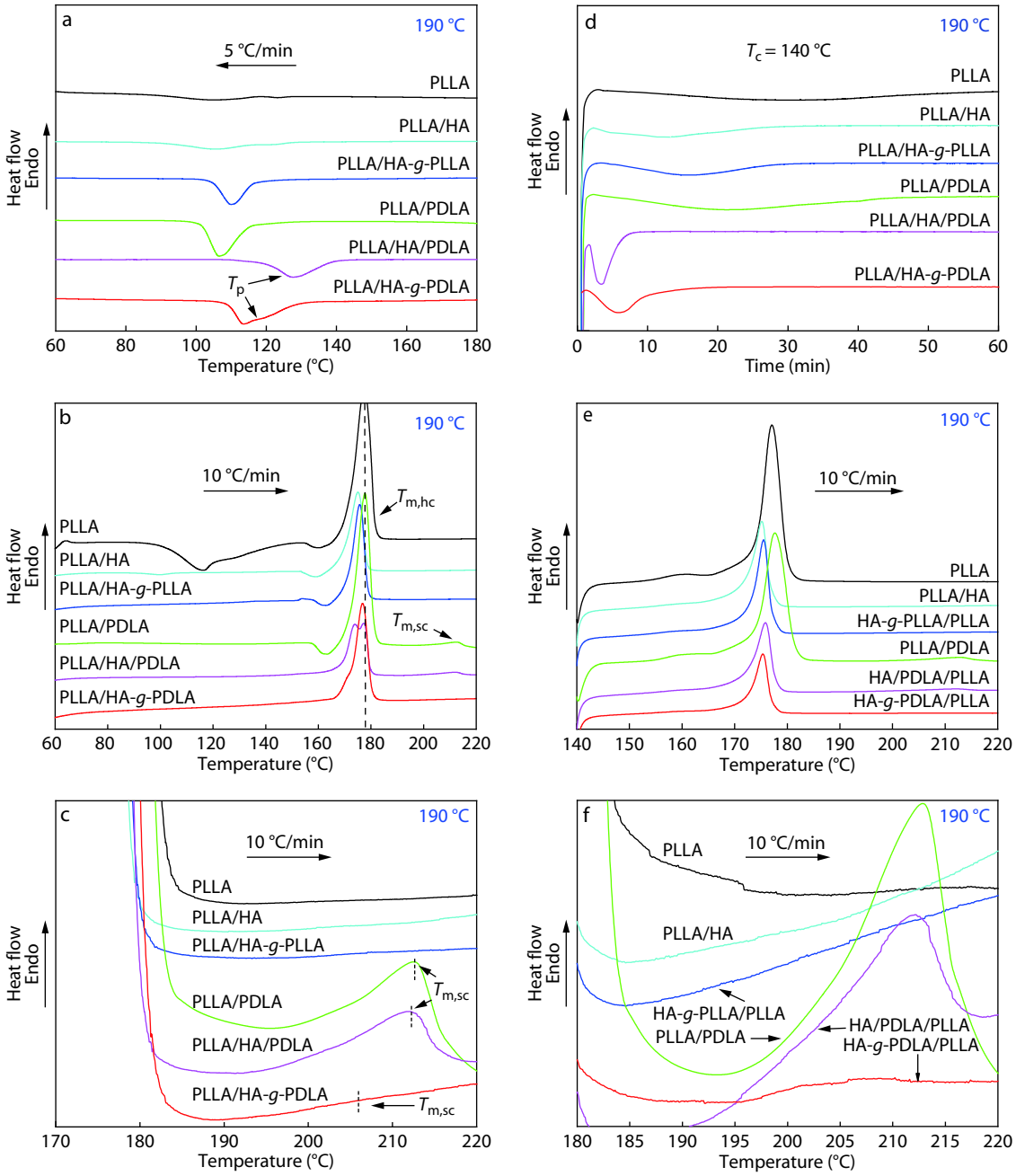

Fig. 3 DSC curves of non-isothermal crystallization, isothermal crystallization and subsequent heating curves of PLLA and its composites when the processing temperature is 190 °C. (a) Cooling curves from 190 °C to 60 °C at a rate of 5 °C/min, (b) subsequent heating curves after non-isothermal crystallization at a rate of 10 °C/min, (c) enlarged curves of (b), (d) isothermal crystallization at 140 °C, (e) subsequent heating curves after isothermal crystallization, (f) enlarged curves of (e).

and 3(c) show the melting curves after crystallization. During non-isothermal crystallization in Fig. 3(a), the crystallization rate increases in the following order: PLLA < PLLA/HA < PLLA/PDLA < PLLA/HA-*g*-PLLA < PLLA/HA-*g*-PDLA < PLLA/HA/PDLA. This order is obtained by comparing the value of the crystallization peak temperature (T_p) of each composite in Fig. 3(a) and Table 2. The crystallization rates of PLLA/HA and PLLA/PDLA composites are faster than that of PLLA, which means the presence of HA particles or SC crystallites can accelerate the PLLA crystallization in these composites. When the HA particles are grafted by PLLA chains, the T_p of PLLA/HA-*g*-PLLA composite increases to 110.0 °C comparing to the PLLA/HA composite, indicating the acceleration effect is improved. The two fastest crystallization rates belong to PLLA/HA/PDLA composite and PLLA/HA-*g*-PDLA composite, because both HA particles and SC crystallites exist in the two composites. This indicates that the combination of HA particles and SC crystallites results in a synergistic effect. In addition, the highest T_p (crystallization peak temperature), which means the fastest crystallization rate, belongs to PLLA/HA/PDLA composite.

https://doi.org/10.1007/s10118-020-2374-1

Table 2 Quantitative analysis on thermal properties of PLLA and its composites during non-isothermal crystallization and subsequent heating process with a processing temperature of 190 °C.

Sample	T_p [a] (°C)	ΔH_c [b] (J/g)	ΔH_{cc} [c] (J/g)	$\Delta H_{m,hc}$ [d] (J/g)	X_c [e] (%)	$T_{m,sc}$ [f] (°C)	$\Delta H_{m,sc}$ [d] (J/g)
PLLA	104.3	−12.9	38.2	64.1	25.2	–	–
PLLA/HA	105.7	−20.3	1.1	27.9	57.0	–	–
PLLA/HA-*g*-PLLA	110.0	−23.4	0	29.6	63.0	–	–
PLLA/PDLA	106.5	−37.1	3.0	49.2	53.5	212.7	3.1
PLLA/PDLA/HA	127.9	−26.8	0	26.1	55.5	212.5	1.3
PLLA/HA-*g*-PDLA	113.9	−24.9	0	36.2	77.0	208.3	0.1

[a] T_p denotes the crystallization peak temperature of the composite in the cooling run. [b] ΔH_c denotes the crystallization enthalpy of the composite in the cooling run. [c] ΔH_{cc} denotes cold crystallization enthalpy of the composite in the second heating run. [d] $\Delta H_{m,hc}$ and $\Delta H_{m,sc}$ denote the fusion enthalpy of homocrystallites and SC crystallites in the second heating run, respectively. [e] $X_c = (\Delta H_{m,hc} - \Delta H_{cc})/(w_f \times \Delta H^0_m)$, w_f is the weight percent of the PLLA matrix, ΔH^0_m = 94 J/g. [f] $T_{m,sc}$ denotes the melting temperature of SC crystallites.

The possible reason is that the PLLA/HA/PDLA composite has more pre-existing SC crystallites than PLLA/HA-*g*-PDLA composite to accelerate PLLA crystallization. This could be confirmed by the $\Delta H_{m,sc}$ values in Fig. 2(a) and these values remain almost unchanged in Fig. 3(c) and Table 2. The crystallinity (X_c) of PLLA in the PLLA composite is much higher than that of neat PLLA (25.2%). This is due to the accelerated crystallization of PLLA during cooling, as more homocrystallites could be formed in the presence of HA particles or PDLA chains.

Fig. 3(a) shows that PLLA homocrystallization begins at 130 °C during the non-isothermal crystallization. As the rapid formation of PLLA homocrystallization at temperatures below 130 °C would restrict PLA stereocomplexation, we selected a higher temperature (140 °C) as the temperature for the isothermal crystallization of PLLA and its different composites. At this temperature it is difficult for homocrystallization, but easier for stereocomplexation.

Fig. 3(d) shows the isothermal crystallization curves of PLLA and its composites when the processing temperature is 190 °C. Figs. 3(e) and 3(f) show the melting curves after isothermal crystallization. The quantitative analyses of the thermal properties of PLLA and its composites during isothermal crystallization and subsequent heating process are tabulated in Table 3. During isothermal crystallization, the crystallization rate increases as follows: PLLA < PLLA/PDLA < PLLA/HA-*g*-PLLA ≈ PLLA/HA < PLLA/HA-*g*-PDLA < PLLA/HA/PDLA. This order is obtained according to the peak time (t_p) values of these composites. The results confirm again that both HA particles and SC crystallites can accelerate the crystallization rate of PLLA. The difference between isothermal crystallization and non-isothermal crystallization is that the crystallization rate of PLLA/HA composite is faster than that of PLLA/PDLA composite in isothermal crystallization, but slower in non-isothermal crystallization. This means that comparing to the PDLA chains in the composite, HA particles can accelerate the crystallization of PLLA at a higher temperature (140 °C) than PDLA chains.

In Table 3, the X_c of each PLLA composite during the isothermal crystallization increases to about 70% comparing to the non-isothermal crystallization in Table 2 when the processing temperature is 190 °C, because there is enough time for PLLA in the composite to crystallize.

Polarized optical microscopy (POM) experiments are carried out in order to investigate the nucleation and the growth of spherulite during isothermal crystallization. Fig. 4 shows the spherulite morphologies and growth rates of PLLA and its composites. It could be seen that the spherulites of neat PLLA are the largest in all the samples (Fig. 4a). When the processing temperature is 190 °C, the addition of HA particles or PDLA in PLLA can significantly increase the number of spherulites (Figs. 4b–4f). Combined with the results in DSC curves in Fig. 3, it can be concluded that the HA particles or SC crystallites in the composites served as nucleation sites accelerating PLLA crystallization. In Fig. 4(g), the spherulite growth rates of the five PLLA composites (PLLA/HA, PLLA/PDLA, PLLA/HA-*g*-PLLA, PLLA/HA-*g*-PDLA, PLLA/HA/PDLA), which are around 5.0 μm/min (Table 4), are close to that of PLLA. Comparing to the increasing number of spherulites in Figs. 4(b)–4(f), the nearly unchanged spherulite growth rate indicates that the acceleration of PLLA crystallization in these composites is primarily due to the increase in nucleating agents rather than spherulite growth rate.

Fig. 5 shows the relative crystallinity (X_t) as a function of crystallization time and the Avrami plots when the processing temperature is 190 °C. In Fig. 5(a), all the curves exhibit a sigmoidal dependence on time. The isothermal crystallization kinetics of PLLA and its composites are analyzed by the Avrami theory. According to the Avrami equation, X_t devel-

Table 3 Quantitative analysis on thermal properties of PLLA and its composites during isothermal crystallization and subsequent heating process with a processing temperature of 190 °C.

Sample	$t_{p,iso}$ [a] (min)	ΔH_c [b] (J/g)	ΔH_{cc} [c] (J/g)	$\Delta H_{m,hc}$ [d] (J/g)	X_c [e] (%)	$T_{m,sc}$ [f] (°C)	$\Delta H_{m,sc}$ [d] (J/g)
PLLA	30.0	−55.7	0	68.3	72.7	–	–
PLLA/HA	13.6	−25.6	0	34.5	73.4	–	–
PLLA/HA-*g*-PLLA	17.1	−29.0	0	34.4	73.2	–	–
PLLA/PDLA	22.6	−67.0	0	67.0	72.9	212.7	3.3
PLLA/PDLA/HA	3.8	−22.8	0	30.2	64.3	208.2	0.7
PLLA/HA-*g*-PDLA	6.2	−25.2	0	34.3	73.0	208.1	0.2

[a] t_p denotes the isothermal crystallization peak time. [b] ΔH_c denotes the crystallization enthalpy of the composite during isothermal crystallization. [c–f] See the footnotes, Table 2.

https://doi.org/10.1007/s10118-020-2374-1

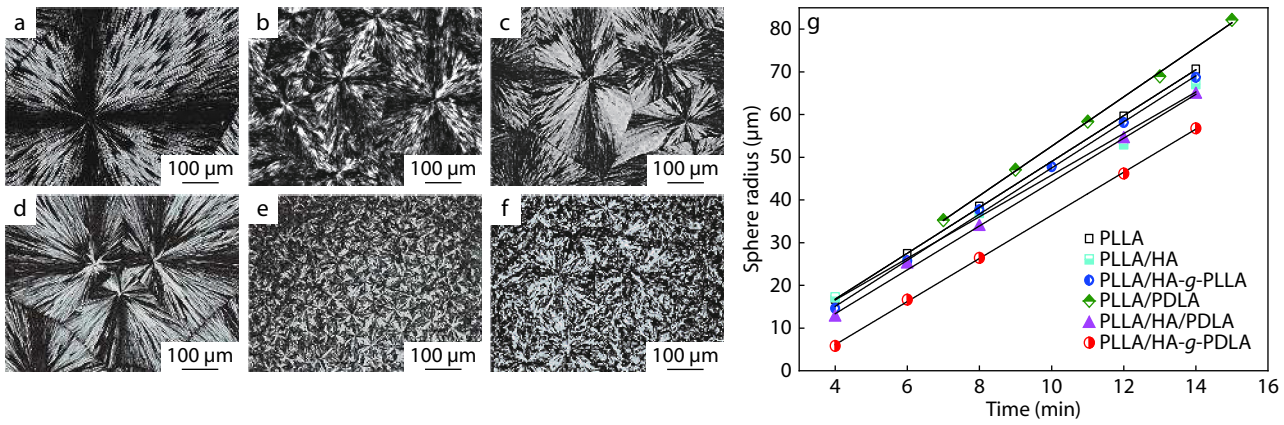

Fig. 4 Polarized optical photomicrographs and radial growth rate of spherulites of PLLA and its composites crystallized isothermally at 140 °C when the processing temperature is 190 °C. (a) PLLA, (b) PLLA/HA, (c) PLLA/HA-*g*-PLLA, (d) PLLA/PDLA, (e) PLLA/HA/PDLA, (f) PLLA/HA-*g*-PDLA, (g) radial growth rate of spherulites.

Table 4 Avrami kinetic parameters for the isothermal crystallization of neat PLLA and its composites at different processing temperatures.

Sample	Processing temperature 190 °C				Processing temperature 230 °C			
	n	k ($\min^{-n}$)	$t_{1/2}$ (min)	G (μm/min)	n	k ($\min^{-n}$)	$t_{1/2}$ (min)	G (μm/min)
PLLA	2.3	2.82×10^{-4}	28.4	5.4	2.1	3.31×10^{-4}	37.8	2.7
PLLA/HA	1.7	9.82×10^{-3}	11.0	4.9	2.1	3.02×10^{-3}	13.5	5.5
PLLA/HA-*g*-PLLA	2.7	5.62×10^{-4}	13.7	5.4	2.6	9.55×10^{-4}	12.8	4.5
PLLA/PDLA	2.3	6.61×10^{-4}	21.3	5.8	2.5	1.51×10^{-4}	27.1	4.0
PLLA/PDLA/HA	2.5	1.26×10^{-2}	5.0	5.1	2.2	2.29×10^{-3}	14.2	5.7
PLLA/HA-*g*-PDLA	3.2	2.97×10^{-3}	5.7	5.1	2.7	3.55×10^{-3}	7.3	5.1

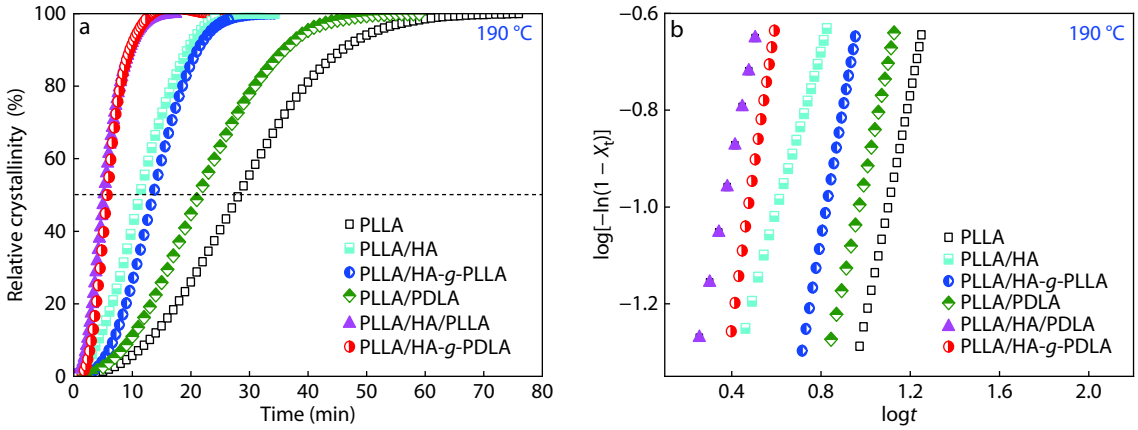

Fig. 5 Plots of (a) relative crystallinity (X_t) versus time and (b) log[−ln(1 − X_t)] versus log$t$ for the isothermal crystallization of PLLA and its composites with a processing temperature of 190 °C (T_c = 140 °C).

ops with t as

$$1 - X_t = \exp(-kt^n) \quad (1)$$

where n is the Avrami exponent depending on the nature of nucleation and growth geometry of the crystals, and k is the overall kinetic rate constant involving both nucleation and growth rate parameters. To avoid deviation from the theoretical curves, X_t was used in the range 3%–20% for estimating n and k. In Fig. 5(b), it is found that all the lines are almost straight and parallel for PLLA and its composites, indicating that the Avrami equation is suitable for describing the overall isothermal melt crystallization process. The related n and k obtained from the slopes and intercepts are listed in Table 4. The values of n for PLLA are about 2.3, which may be related to one-dimensional (fibrillar) growth with a homogeneous nucleation crystallization mechanism.[30] Jiang *et al.* reported that the value of n increased a little in HA/PLGA composite compared with neat PLGA due to large numbers of crystal HA nucleus.[31] However, in our study the value of n for PLLA/HA composite is reduced to 1.7 when the processing temperature is 190 °C. Combined with the accelerating rate of PLLA crystallization in this composite in isothermal crystallization, the reduced n values suggested that high content of HA particles in the composite may restrict crystal growth. When PDLA chains are introduced into the blend of PLLA and PDLA, because of the synergistic effect of HA

particles and SC crystallites on the acceleration of PLLA crystallization, *n* value of PLLA/HA/PDLA composite increases to 2.5 when the processing temperature is 190 °C. Furthermore, when PLLA or PDLA chains are grafted onto HA particles, the value of *n* increases to 2.6 or higher. The *n* value of HA-*g*-PDLA/PLLA composite even increases to 3.2; this significant increase in *n* demonstrates that the nucleation mechanism and the morphology of crystal growth change from one-dimensional (fibrillar) growth with a homogeneous nucleation mode to two-dimensional (circular) or three-dimensional (spherical) growth with a heterogeneous nucleation mode.

Processing Temperature above T_{mz} of SC Crystallites

Non-isothermal crystallization and isothermal crystallization after melting at 230 °C are investigated in Fig. 6. The quantitative analyses of the thermal properties of PLLA and its composites during crystallization and subsequent heating process are tabulated in Table 5 and Table 6.

Fig. 6(a) shows the non-isothermal crystallization curves of PLLA and its composites when the processing temperature is 230 °C. Figs. 6(b) and 6(c) show the subsequent melting

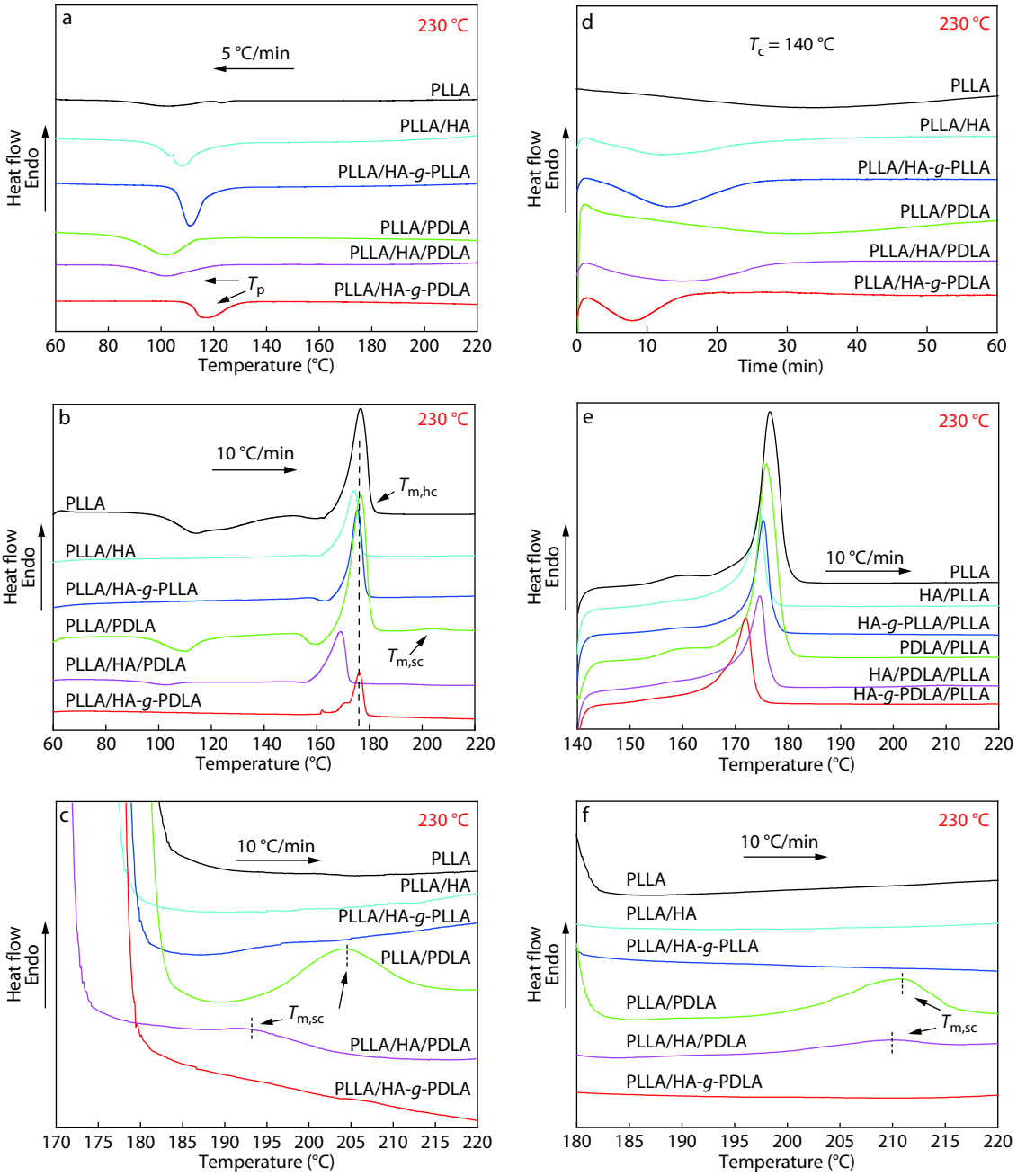

Fig. 6 DSC curves of non-isothermal crystallization, isothermal crystallization and subsequent heating curves of PLLA and its composites after melting at 230 °C. (a) Cooling curves from 230 °C to 60 °C at a rate of 5 °C /min, (b) subsequent heating curves after non-isothermal crystallization at a rate of 10 °C/min, (c) enlarged curves of (b), (d) isothermal crystallization at 140 °C, (e) subsequent heating curves after isothermal crystallization, (f) enlarged curves of (e).

https://doi.org/10.1007/s10118-020-2374-1

Table 5 Quantitative analysis on thermal properties of PLLA and its composites during non-isothermal crystallization and subsequent heating process with a processing temperature of 230 °C.

Sample	T_p [a] (°C)	ΔH_c [b] (J/g)	ΔH_{cc} [c] (J/g)	$\Delta H_{m,hc}$ [d] (J/g)	X_c [e] (%)	$T_{m,sc}$ [f] (°C)	$\Delta H_{m,sc}$ [d] (J/g)
PLLA	102.0	−9.4	29.7	46.7	18.1	–	–
PLLA/HA	107.9	−23.5	1.0	25.8	54.8	–	–
PLLA/HA-*g*-PLLA	110.8	−24.4	0	27.8	59.1	–	–
PLLA/PDLA	101.3	−20.2	14.4	50.4	39.2	204.0	1.4
PLLA/PDLA/HA	102.6	−15.2	3.4	22.8	41.3	204.9	0.2
PLLA/HA-*g*-PDLA	118.5	−13.7	0	14.1	30.0	–	–

[a–f] See the footnotes, Table 2.

Table 6 Quantitative analysis on thermal properties of PLLA and its composites during isothermal crystallization and subsequent heating process with a processing temperature of 230 °C.

Sample	$t_{p,iso}$ [a] (min)	ΔH_c [b] (J/g)	ΔH_{cc} [c] (J/g)	$\Delta H_{m,hc}$ [d] (J/g)	X_c [e] (%)	$T_{m,sc}$ [f] (°C)	$\Delta H_{m,sc}$ [d] (J/g)
PLLA	35.0	−64.8	0	62.4	66.4	–	–
PLLA/HA	13.8	−26.3	0	33.3	70.9	–	–
PLLA/HA-*g*-PLLA	13.0	−33.7	0	34.2	72.8	–	–
PLLA/PDLA	31.2	−59.8	0	63.6	69.2	210.8	2.3
PLLA/PDLA/HA	16.0	−28.3	0	34.8	74.0	209.1	0.5
PLLA/HA-*g*-PDLA	8.6	−16.0	0	21.3	45.3	–	–

[a–f] See the footnotes, Table 3.

curves after crystallization. The crystallization rate during non-isothermal crystallization increases as follows: PLLA < PLLA/PDLA < HA/PDLA/PLLA < PLLA/HA ≈ PLLA/HA-*g*-PLLA < PLLA/HA-*g*-PDLA. This order is obtained according to the T_p values in Fig. 6(a) and Table 5. It can be seen that when the processing temperature increases from 190 °C to 230 °C, the crystallization rate of PLLA in PLLA/HA and PLLA/HA-*g*-PLLA composites is still accelerated by the presence of HA particles and PLLA-grafted HA particles, respectively. However, the crystallization rates of PLLA/HA/PDLA and PLLA/PDLA composite containing SC crystallites decrease dramatically comparing to those when the processing temperature is 190 °C in Fig. 3(a) and Table 2, because the SC crystallites melt completely with this processing temperature, and they have to recrystallize during the non-isothermal crystallization, resulting in the reduced acceleration effect for PLLA crystallization. After the recrystallization, the number of SC crystallites formed in the composites decreases, which is confirmed by the reduction of $\Delta H_{m,sc}$ values (1.4 J/g for PLLA/PDLA composite, 0.2 J/g for PLLA/HA/PDLA composite, and 0 J/g for PLLA/PLLA-*g*-PDLA composite) in Table 5. However, the crystallization of PLLA/HA-*g*-PDLA composite is not significantly affected by the melting of SC crystallites in it, which is different from other composites containing SC crystallites, and it owns the highest T_p among all the samples. We suggest that comparing to the PDLA chains dispersed between the HA particles in PLLA/HA/PDLA composite, the PDLA chains grafted onto the HA particles in PLLA/HA-*g*-PDLA composite are easier to interact with PLLA chains to form nucleation sites, because the HA particles in the composite can attract PLLA chains to their surface. At the same time, the T_p of PLLA/HA-*g*-PDLA composite is higher than that of PLLA/HA-*g*-PLLA, and the subsequent heating curve shows that there are no SC crystallites in the PLLA/HA-*g*-PDLA composite (Fig. 6f), so we suggest that the interaction between the grafted PDLA chains and the amorphous PLLA chains (PDLA-PLLA interaction) is better in promoting the crystallization of PLLA in the composite than PLLA-PLLA interaction in the PLLA/HA-*g*-PLLA composite. The X_cs of the composites containing PDLA chains decrease as compared with those when the processing temperature is 190 °C. The reason for this is the competition between homocrystallization and stereocomplexation. The X_c of PLLA/HA-*g*-PDLA is the lowest (30.0%) of the three composites, suggesting that the grafted PDLA chains are more free at the melting temperature of 230 °C, which is higher than the melting temperature of the SC crystallites in the composite. Combining with the fact that HA particles disperse best in PLLA/HA-*g*-PDLA composite (Fig. S1 in ESI), more grafted PDLA chains can interact with the amorphous PLLA chains. However, as the content of PDLA is very low, the SC crystallites are difficult to be formed. We suggest that there may be a "mesophase" before the formation of SC crystallites because of the PLLA-PDLA interaction.[32] These mesophase PLLA-PDLA aggregates are easier to accelerate the crystallization of PLLA chains which are around them in the melt state, however difficult to form SC crystallites, because they are distributed separately around the HA particles. This may be the reason why there were fewer or no SC crystallites after melt-crystallization when the processing temperature is 230 °C.

Fig. 6(d) shows the isothermal crystallization curves of PLLA and its composites when the processing temperatures is 230 °C. Figs. 6(e) and 6(f) show the subsequent melting curves after isothermal crystallization. During isothermal crystallization, the crystallization rate increases as follows: PLLA < PLLA/PDLA < HA/PDLA/PLLA < PLLA/HA-*g*-PLLA ≈ PLLA/HA < PLLA/HA-*g*-PDLA (t_ps are 35.0, 31.2, 16.0, 13.8, 13.0, and 8.6 min, respectively). The order of crystallization rate is similar to that of the non-isothermal crystallization. In Fig. 6(f), it is worth noting that there is still no melting peak of SC crystallites in the melting curve of PLLA/HA-*g*-PDLA composite after isothermal crystallization as it is in the non-isothermal crystallization in Fig. 6(c). This result confirms again that even there are no SC crystallites formed in the composite, the acceleration effect of HA-*g*-PDLA on PLLA crystallization is the best in the five PLLA composites.

Fig. 7 shows the spherulite morphologies and growth rates

of PLLA and its composites when the processing temperature is 230 °C. Comparing to the spherulite morphologies of PLLA in Fig. 7(a), the number of the spherulites in Figs. 7(b)–7(f) increase, which means that HA particles, PDLA chains, and PLA grafted HA particles can act as nucleators for the PLLA crystallization, and these morphologies are similar to those in Fig. 4. However, when we compare the spherulite morphologies in Fig. 7(e) with those in Fig. 4(e), the number of spherulites of HA/PDLA/PLLA in Fig. 7(e) decreases dramatically, indicating again that when the SC crystallites were melted in the HA/PDLA/PLLA composite, it would be difficult to form SC crystallites to accelerate the crystallization of PLLA. At the same time, the number of PLLA/HA-*g*-PDLA in Fig. 7(f) does not decrease so much comparing to that in Fig. 4(f) but still maintains good acceleration effect for PLLA. Although the SC crystallites were also melted in PLLA/HA-*g*-PDLA composite at a processing temperature of 230 °C, HA particles grafted by PDLA chains can still form nucleation sites to accelerate PLLA crystallization. The spherulite growth rate of PLLA in Fig. 7(a) decreases significantly (from 5.4 μm/min to 2.0 μm/min), which may because the higher melting temperature reduces the density of aggregates in the melt.[33] There is not much change of the spherulite growth rate for the five composites.

Fig. 8 shows the relative crystallinity (X_t) as a function of crystallization time and the Avrami plots when the processing temperature is 230 °C. The Avrami kinetic parameters are listed in Table 4. Comparing to those when the processing temperature is 190 °C, the n values remain about 2.1–2.7, indicating there is no great change for the nucleation mechanism and the morphology of crystal growth for the PLLA composites.

Crystallization Mechanism of PLLA/HA-*g*-PDLA Composite

Based on the above discussion, the accelerating mechanism of the modified HA particles on the crystallization of PLLA in the composite is explained as follows. When the processing temperature is 190 °C, the SC crystallites and HA particles both can accelerate PLLA homocrystallization, resulting in a synergistic effect. On the other hand, when the processing temperature rises to 230 °C, the SC crystallites melt completely (Fig. 9a); however, the grafted PDLA chains may attract the molten PLLA chains to the surface of the PLA-grafted HA particles by the PDLA-PLLA interaction (Fig. 9b). So, even there are few or no SC crystallites formed under this condition, HA-*g*-PDLA can still accelerate PLLA homocrystallization (Fig. 9c).

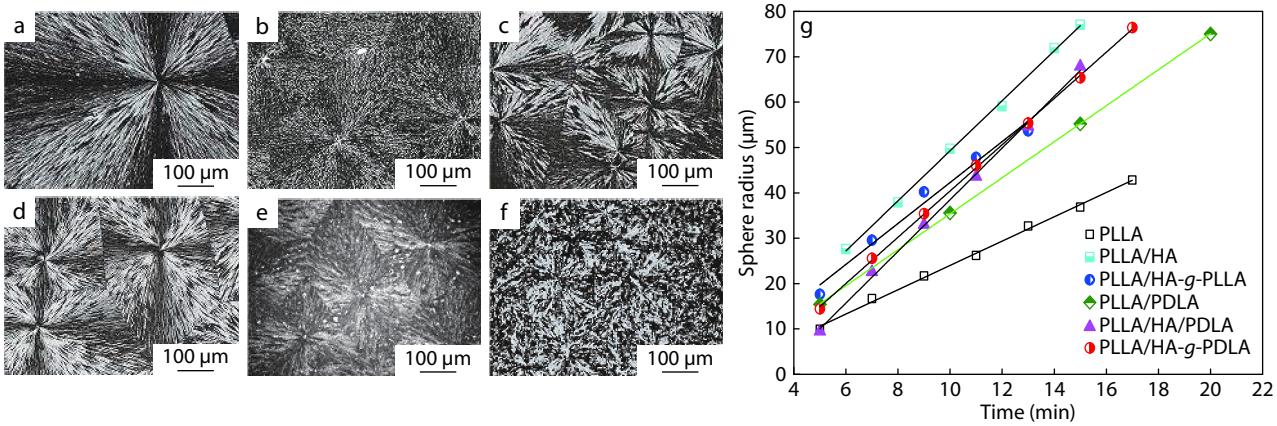

Fig. 7 Polarized optical photomicrographs and radial growth rate of spherulites of PLLA and its composites crystallized isothermally at 140 °C when the processing temperature is 230 °C. (a) PLLA, (b) PLLA/HA, (c) PLLA/HA-*g*-PLLA, (d) PLLA/PDLA, (e) PLLA/HA/PDLA, (f) PLLA/HA-*g*-PDLA, (g) radial growth rate of spherulites.

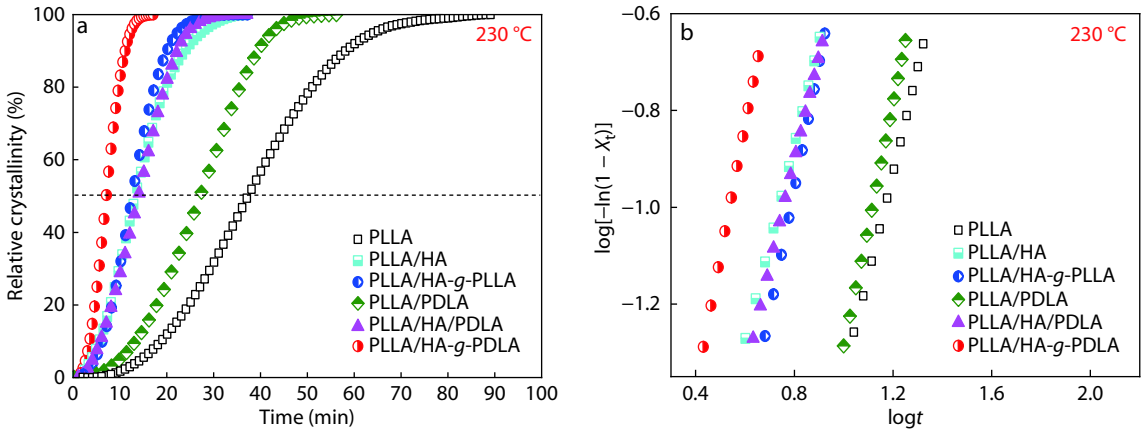

Fig. 8 Plots of (a) relative crystallinity (X_t) versus time and (b) log[−ln(1 − X_t)] versus log$t$ for the isothermal crystallization of PLLA and its composites with a processing temperature of 230 °C (T_c = 140 °C).

https://doi.org/10.1007/s10118-020-2374-1

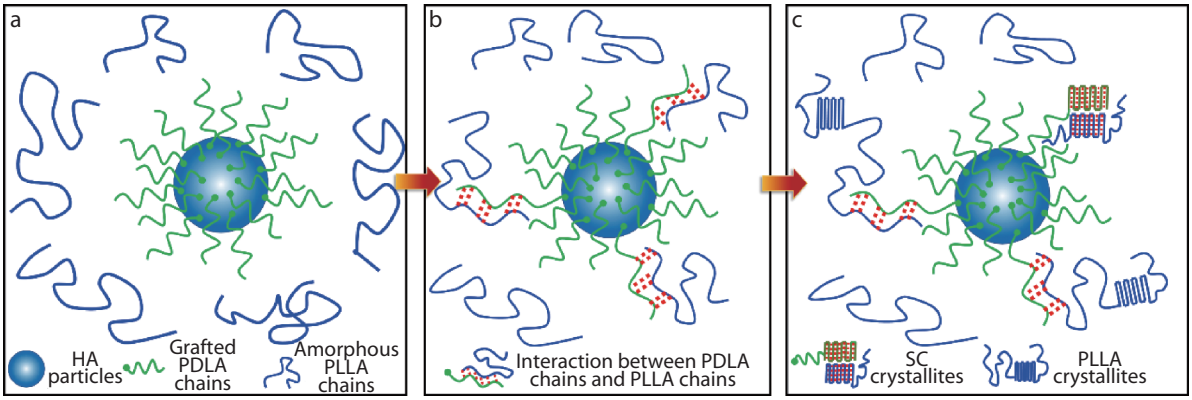

Fig. 9 The accelerating mechanism of the HA-*g*-PDLA on the crystallization of PLLA at the processing temperature of 230 °C.

CONCLUSIONS

In this study, HA-*g*-PDLA was synthesized by *in situ* polymerization of DLA to HA particles. The crystallization behavior of PLLA/HA-*g*-PDLA was investigated with different processing temperatures comparing to the composites of PLLA/HA, PLLA/HA-*g*-PLLA, HA/PDLA/PLLA and PLLA/PDLA. It was found that both HA particles and SC crystallites could act as accelerating agent for PLLA crystallization when the processing temperature was 190 °C. As a result, the crystallization rates of all the composites were faster than that of neat PLLA. HA/PDLA/PLLA composite had the fastest crystallization rate because of the synergetic effect of HA particles and SC crystallites. However, when the processing temperature rose to 230 °C, the accelerating effect of SC crystallites in this composite dramatically decreased, because the SC crystallites melted at this temperature and would reform during the crystallization process, resulting in a competitive effect between homocrystallization and stereocomplexation. Interestingly, the accelerating effect of HA-*g*-PDLA did not drop so much as other composites containing SC crystallites at the processing temperature of 230 °C. The possible reasons are as follows. First, few or no SC crystallites were formed because PDLA chains were grafted onto HA particles, so there was less competition between SC crystallization and homocrystallization during recrystallization. Second, the grafted PDLA chains may interact with the amorphous PLLA chains in the composite to form nucleation sites for PLLA crystallization. Compared to other composites, the PLLA nucleation mechanism and the crystal growth form were more likely to be three-dimensional (spherical) growth with heterogeneous nucleation mode.

Electronic Supplementary Information

Electronic supplementary information (ESI) is available free of charge in the online version of this article at http://dx.doi.org/10.1007/s10118-020-2374-1.

ACKNOWLEDGMENTS

This work was financially supported by the National Natural Science Foundation of China (Nos. 51603005 and 51973010) and Beijing Natural Science Foundation (No. 2182052).

REFERENCES

1 Jain, A.; Kunduru, K. R.; Basu, A.; Mizrahi, B.; Domb, A. J.; Khan, W. Injectable formulations of poly(lactic acid) and its copolymers in clinical use. *Adv. Drug Deliver. Rev.* **2016**, *107*, 213–227.
2 Du, N.; Guo, W. X.; Yu, Q. S.; Guan, S. L.; Guo, L. Y.; Shen, T.; Tang, H.; Gan, Z. H. Poly(D,L-lactic acid)-block-poly(*N*-(2-hydroxypropyl) methacrylamide) nanoparticles for overcoming accelerated blood clearance and achieving efficient anti-tumor therapy. *Polym. Chem.* **2016**, *7*, 5719–5729.
3 Phetwarotai, W.; Tanrattanakul, V.; Phusunti, N. Synergistic effect of nucleation and compatibilization on the polylactide and poly(butylene adipate-*co*-terephthalate) blend films. *Chinese J. Polym. Sci.* **2016**, *34*, 1129–1140.
4 Ma, C. L.; Pan, P. J.; Shan, G. R.; Bao, Y. Z.; Fujita, M.; Maeda, M. Core-shell structure, biodegradation, and drug release behavior of poly(lactic acid)/poly(ethylene glycol) block copolymer micelles tuned by macromolecular stereostructure. *Langmuir* **2015**, *31*, 1527–1536.
5 Binan, L.; Tendey, C.; de, Crescenzo G.; El, Ayoubi R.; Ajji, A.; Jolicoeur, M. Differentiation of neuronal stem cells into motor neurons using electrospun poly-L-lactic acid/gelatin scaffold. *Biomaterials* **2014**, *35*, 664–674.
6 Wang, Z. L.; Wang, Y.; Ito, Y.; Zhang, P. B.; Chen, X. S. A comparative study on the *in vivo* degradation of poly(L-lactide) based composite implants for bone fracture fixation. *Sci. Rep.* **2016**, *6*, 20770.
7 Fambri, L.; Pegoretti, A.; Fenner, R.; Incardona, S.; Migliaresi, C. Biodegradable fibres of poly(L-lactic acid) produced by melt spinning. *Polymer* **1997**, *38*, 79–85.
8 Tsuji, H.; Takai, H.; Saha, S. K. Isothermal and non-isothermal crystallization behavior of poly(L-lactic acid): effects of stereocomplex as nucleating agent. *Polymer* **2006**, *47*, 3826–3837.
9 Schmidt, S. C.; Hillmyer, M. A. Polylactide stereocomplex crystallites as nucleating agents for isotactic polylactide. *J. Polym. Sci., Part B: Polym. Phys.* **2001**, *39*, 300–313.
10 Xu, J. Z.; Zhang, Z. J.; Xu, H.; Chen, J. B.; Ran, R.; Li, Z. M. Highly enhanced crystallization kinetics of poly(L-lactic acid) by poly(ethylene glycol) grafted graphene oxide simultaneously as heterogeneous nucleation agent and chain mobility promoter. *Macromolecules* **2015**, *48*, 4891–4900.
11 Song, L. Y.; Sun, L.; Jiang, N.; Gan, Z. H. Structural control and hemostatic properties of porous microspheres fabricated by

hydroxyapatite-graft-poly(D,L-lactide) nanocomposites. *Compos. Sci. Technol.* **2016**, *134*, 234–241.
12 Zhou, S. B.; Zheng, X. T.; Yu, X. J.; Wang, J. X.; Weng, J.; Li, X. H.; Feng, B.; Yin, M. Hydrogen bonding interaction of poly(D,L-lactide)/hydroxyapatite nanocomposites. *Chem. Mater.* **2007**, *19*, 247–253.
13 Cui, W.; Li, X.; Zhou, S.; Weng, J. *In situ* growth of hydroxyapatite within electrospun poly(D,L-lactide) fibers. *J. Biomed. Mater. Res., Part A* **2007**, *82A*, 831–841.
14 Wan, Y. Z.; Wu, C. Q.; Xiong, G. Y.; Zuo, G. F.; Jin, J.; Ren, K. J.; Zhu, Y.; Wang, Z. R.; Luo, H. L. Mechanical properties and cytotoxicity of nanoplate-like hydroxyapatite/polylactide nanocomposites prepared by intercalation technique. *J. Mech. Behav. Biomed.* **2015**, *47*, 29–37.
15 Wei, J. C.; Sun, J. R.; Wang, H. J.; Chen, X. S.; Jing, X. B. Isothermal crystallization behavior and unique banded spherulites of hydroxyapatite/poly(L-lactide) nanocomposites. *Chinese J. Polym. Sci.* **2010**, *28*, 499–507.
16 Liu, Z.; Chen, Y. H.; Ding, W. W.; Zhang, C. H. Filling behavior, morphology evolution and crystallization behavior of microinjection molded poly(lactic acid)/hydroxyapatite nanocomposites. *Compos. Part A-Appl. S.* **2015**, *72*, 85–95.
17 Li, J.; Zheng, W.; Zheng, Y. F.; Lou, X. Cell responses and hemocompatibility of *g*-HA/PLA composites. *Sci. China-Life Sci.* **2011**, *54*, 366–371.
18 Li, J.; Lu., X. L.; Zheng Y. F. Effect of surface modified hydroxyapatite on the tensile property improvement of HA/PLA composite. *Appl. Surf. Sci.* **2008**, *255*, 494–497.
19 Wang, T. X.; Chow, L. C.; Frukhtbeyn, S. A.; Ting, A. H.; Dong, Q. X.; Yang, M. S.; Mitchell, J. W. Improve the strength of PLA/HA composite through the use of surface initiated polymerization and phosphonic acid coupling agent. *J. Res. Natl. Inst. Stand. Technol.* **2011**, *116*, 785–796.
20 Qiu, X. Y.; Hong, Z. K.; Hu, J. L.; Chen, L.; Chen, X. S.; Jing, X. B. Hydroxyapatite surface modified by L-lactic acid and its subsequent grafting polymerization of L-lactide. *Biomacromolecules* **2005**, *6*, 1193–1199.
21 Huang, G. M.; Du, Z. Y.; Yuan, Z. Y.; Gu, L. H.; Cai, Q.; Yang, X. P. Poly(L-lactide) nanocomposites containing poly(D-lactide) grafted nanohydroxyapatite with improved interfacial adhesion *via* stereocomplexation. *J. Mech. Behav. Biomed.* **2018**, *78*, 10–19.
22 Narita, J.; Katagiri, M.; Tsuji, H. Highly enhanced nucleating effect of melt-recrystallized stereocomplex crystallites on poly(L-lactic acid) crystallization. *Macromol. Mater. Eng.* **2011**, *296*, 887–893.
23 Yamane, H.; Sasai, K. Effect of the addition of poly(D-lactic acid) on the thermal property of poly(L-lactic acid). *Polymer* **2003**, *44*, 2569–2575.
24 Chang, M. C.; Tanaka, J. FTIR study for hydroxyapatite/collagen nanocomposite cross-linked by glutaraldehyde. *Biomaterials* **2002**, *23*, 4811–4818.
25 Hong, Z. K.; Qiu, X. Y.; Sun, J. R.; Deng, M. X.; Chen, X. S.; Jing, X. B. Grafting polymerization of L-lactide on the surface of hydroxyapatite nano-crystals. *Polymer* **2004**, *45*, 6699–6706.
26 Bahrololoom, M. E.; Javidi, M.; Javadpour, S.; Ma, J. Characterisation of natural hydroxyapatite extracted from bovine cortical bone ash. *J. Ceram. Process. Res.* **2009**, *10*, 129–138.
27 Borum-Nicholas, L.; Wilson, O. Surface modification of hydroxyapatite. Part I. Dodecyl alcohol. *Biomaterials* **2003**, *24*, 3671–3679.
28 Sun, Y.; He, C. B. Synthesis and stereocomplex crystallization of poly(lactide)-graphene oxide nanocomposites. *ACS Macro. Lett.* **2012**, *1*, 709–713.
29 Narita, J.; Katagiri, M.; Tsuji, H. Highly enhanced accelerating effect of melt-recrystallized stereocomplex crystallites on poly(L-lactic acid) crystallization: effects of molecular weight of poly(D-lactic acid). *Polym. Int.* **2013**, *62*, 936–948.
30 Nouri, S.; Dubois, C.; Lafleur, P. G. Homocrystal and stereocomplex formation behavior of polylactides with different branched structures. *Polymer* **2015**, *67*, 227–239.
31 Jiang, L. Y.; Xiong, C. D.; Jiang, L. X.; Xu, L. J. Effect of hydroxyapatite with different morphology on the crystallization behavior, mechanical property and *in vitro* degradation of hydroxyapatite/poly(lactic-*co*-glycolic) composite. *Compos. Sci. Technol.* **2014**, *93*, 61–67.
32 Yang, C. F.; Huang, Y. F.; Ruan, J.; Su, A. C. Extensive development of precursory helical pairs prior to formation of stereocomplex crystals in racemic polylactide melt mixture. *Macromolecules* **2012**, *45*, 872–878.
33 Li, X. Y.; Liu, Y. P.; Tian, X. Y.; Cui, K. P. Molecular mechanism leading to memory effect of mesomorphic isotactic polypropylene. *J. Polym. Sci., Part B: Polym. Phys.* **2016**, *54*, 1573–1580.

https://doi.org/10.1007/s10118-020-2374-1